applied sciences

MDPI

Article

Investigation into the Time-Dependent Characteristics of Stress and Deformation of Weak Surrounding Rock and Lining Structure in Operational Tunnels: Model Test

Pai Wang [1], Xujin Ma [2], Lei Yang [1,*], Xiangchao Sheng [1], Xiaolong Wang [1] and Chunjin Lin [1]

[1] Geotechnical and Structural Engineering Research Center, Shandong University, Jinan 250061, China; paiwang@mail.sdu.edu.cn (P.W.); shengxc@mail.sdu.edu.cn (X.S.); xlw241323@163.com (X.W.); linchunjin@sdu.edu.cn (C.L.)
[2] Hubei Provincial Tendering Co., Ltd., Wuhan 430077, China; maxujin3079@csadi.cn
* Correspondence: yanglei@sdu.edu.cn

Abstract: During the long-term operation of tunnels, surrounding rock undergoes creep effects under environmental loads, resulting in changes in the aging evolution model of stress and deformation in surrounding rock and lining, which affects the long-term operational safety of the tunnel. Therefore, using the model test device for time-dependent characteristics of stress and deformation of weak surrounding rock and lining structure in operational tunnels, taking into account the influence of tunnel burial depth and lateral pressure coefficient of surrounding rock, a model test on time-dependent characteristics of stress and deformation in weak surrounding rock and lining structure was conducted, and the stress and deformation time-varying curves at key locations of surrounding rock and lining were obtained. The time characteristics of surrounding rock stress, the contact force between surrounding rock and lining, internal force, and displacement of lining structure were analyzed. Research findings indicate that the stress of surrounding rock, the internal force and displacement of lining structure, and the contact force between surrounding rock and lining all increase and tend to be stable over time under constant load. This implies that the stress and deformation of the surrounding rock and lining structure exhibit time-dependent changes. With changes in burial depth and lateral pressure coefficient, significant variations are observed in the various indicators of stress and deformation in the surrounding rock and lining structure, indicating both time-dependent and long-term characteristics in terms of stress and deformation. The research results provide basic data support for the study of the time-dependent characteristics of stress and deformation between weak surrounding rock and lining structures in operational tunnels and can provide theoretical and technical guidance for the long-term service status discrimination and disaster prevention and control of operational tunnels.

Keywords: creep effect; operational tunnel; stress and deformation of surrounding rock and lining; model test; time-dependent characteristics

check for updates

Citation: Wang, P.; Ma, X.; Yang, L.; Sheng, X.; Wang, X.; Lin, C. Investigation into the Time-Dependent Characteristics of Stress and Deformation of Weak Surrounding Rock and Lining Structure in Operational Tunnels: Model Test. *Appl. Sci.* **2024**, *14*, 5447. https://doi.org/10.3390/app14135447

Academic Editor: Asterios Bakolas

Received: 15 May 2024
Revised: 15 June 2024
Accepted: 18 June 2024
Published: 23 June 2024

Copyright: © 2024 by the authors. Licensee MDPI, Basel, Switzerland. This article is an open access article distributed under the terms and conditions of the Creative Commons Attribution (CC BY) license (https://creativecommons.org/licenses/by/4.0/).

1. Introduction

Numerous tunnels are being implemented in the highway, railroad, and municipal domains as the scope of tunnel and subterranean engineering work keeps growing. According to statistics, China has opened 21,055 km of railroad tunnels, 9691 km of subways, and 21,999 km of highway tunnels [1,2]. Tunnel traffic in a variety of fields has also transitioned from the high-speed construction phase to the comprehensive operation and maintenance phase. China has complicated geological conditions, with many tunnels passing through soft ground. During the tunnel operation process, the soft surrounding rock's creep effect causes the surrounding rock and lining structure to deform in a complex way over time. This deformation has become a crucial factor affecting the tunnel structure's long-term safety. The soft surrounding rock causes creep effects when environmental loads act on

it. This causes the lining structure to be unable to withstand the increasing pressure of the surrounding rock, which can result in lining deformation, cracking, or even failure, among other issues that have a direct impact on the tunnel lining structure's long-term safety. There are clear time-dependent characteristics in the stress and deformation of the tunnel's surrounding rock and lining structure, and these features vary depending on the operating stage. Research on time-dependent characteristics is therefore very important from a theoretical and practical point of view to identify the service state and to prevent and control diseases.

Many academics are currently conducting extensive research on the stress and deformation properties of the surrounding rock and lining. According to Liu et al.'s theoretical research [3], there is a complicated connection between the lining structure and the surrounding rock, and by modifying the lining structure's deformation, the surrounding rock's stress and energy release can be controlled. The elasticity analysis of the non-hydrostatic stress field in the two scenarios of complete and smooth contact between the surrounding rock and lining resolution has been explored by Einstein et al. [4], Yu et al. [5], Li et al. [6], Lu et al. [7], and Caeeanza et al. [8]. The interaction mechanism between the tunnel lining and surrounding rock has been the subject of systematic studies by Fang et al. [9], Zhou et al. [10], Lu et al. [11], and Zhao et al. [12].

In terms of experimental research, Du et al. [13] considered the impact of the post-lining cavity on the interaction between the surrounding rock and lining and conducted an indoor modeling test in the case of the Wushan Tunnel, analyzing the position and size of the post-lining cavity on the structural stability of the tunnel. Xu et al. [14] conducted research and development as well as the formulation of similar materials for surrounding rock and lining, on the basis of which they conducted research on the cracking mechanism of tunnel lining crack damage and the characteristic law of the physical field response of the tunnel surrounding rock and lining structure. Wu et al. [15] and Hu et al. [16] studied the stress and deformation characteristics of surrounding rock and lining structure under bias conditions by taking into account the influence of adverse geological conditions on tunnels, whereas Yang et al. [17] and Sheng et al. [18] considered the impact of water on the surrounding rock. Cui et al. [19] and Wang et al. [20] conducted indoor model tests on the mechanical behavior of lining based on specific tunnel projects to investigate the bearing characteristics of new concrete lining under a weak surrounding rock environment. Qiu et al. [21], Li et al. [22], and Zhou et al. [23] took into consideration the influence of the excavation method and support parameters, carried out indoor model tests, and conducted a systematic and in-depth study on the deformation and force characteristics of the surrounding rock and lining structure after excavation and support.

In numerical simulation research, Ma et al. [24], Liu et al. [25], and Lu et al. [26] combined numerical simulation with the real needs of a tunnel project to study the influence of lining method and important lining parameters on the overall safety of the tunnel. A proposed method for calculating the common bearing capacity is given. The interaction and force deformation characteristics of the tunnel's surrounding rock and lining structure were studied by Jia et al. [27] and Ren et al. [28] using finite element software. The accuracy of the numerical calculation method was confirmed by comparing it with theoretical analyses and on-site measurements. Ren et al. [29] used finite difference software to study the mechanical model of the imperfect interface between the surrounding rock lining and its analytical method to improve the force mechanism of the contact interface and to propose a method of determining the common bearing capacity of the surrounding rock-lining system. Fan et al. [30] investigated the damage and rupture mechanism of the shallow tunnel's lining using discrete element software and summarized the assessment process for the lining's impact on the tunnel's stability support.

The stress and deformation properties of the surrounding rock and lining structure are currently the subject of much domestic and international research, yielding many novel findings. However, the following issues persist: lack of research on the tunnel's operation period results in an unclear evolution law for the stress and deformation of the surrounding

rock and lining during long-term tunnel maintenance and makes it challenging to accurately predict operational diseases. Research on the stress and deformation characteristics of the surrounding rock and lining structure is primarily taken into consideration during the tunnel's construction. Because of this, it is difficult to forecast operational diseases, and it is uncertain how the surrounding rock and lining will change in terms of stress and deformation during long-term tunnel operation and maintenance.

Theoretical analysis, numerical simulation, and model test are the main methods to study the time-dependent characteristics of stress and deformation of tunnel surrounding rock and lining structure, among which, the physical model test can more accurately reflect the stress and deformation characteristics and can provide fundamental data support for clarifying the time-dependent evolution mechanism of stress and deformation. Given the pressing need for the long-term operation and maintenance safety of subterranean projects and tunnels, as well as the deficiencies in the current body of research, this study employs a physical model test method to investigate the time-dependent characteristics of stress and deformation of weak surrounding rock and lining structure in operational tunnels. Additionally, the study aims to clarify the time-dependent evolution mode of stress and deformation of surrounding rock and lining structure and analyze the impact of varying burial depths and lateral pressure coefficients on these parameters. The relevant results can offer theoretical references for determining the operational tunnels' long-term service state as well as for preventing and controlling disasters.

2. Experimental Outline

2.1. Model Test Similarity Criteria and Material Preparation

The basic project for this study is Qingdao Metro Line 6, with a tunnel depth of 10.3–18.8 m. The tunnel's lining measures 6 m in OD and 5.4 m in ID. It primarily travels through weak and unstable fully to moderately worn diorite, where the creep effect is clearly visible. Consequently, the medium-weathering diorite is chosen as the prototype surrounding rock in this paper's physical model test. Similar materials for the surrounding rock and lining are then prepared and chosen based on a similarity criterion. Finally, research is conducted on the time-dependent characteristics of the surrounding rock and lining structure of the operational tunnel stress and deformation.

The fundamental similarity ratios used in the model test are the geometric similarity ratio ($C_L = 30$) and the unit weight similarity ratio ($C_\gamma = 1$), and the similarity ratio between the prototype value and the model value of each physicomechanical parameter is derived according to the principle of the similarity theory: the similarity ratio of Poisson's ratio, strain, and angle of internal friction is 1 ($C_\mu = C_\varepsilon = C_\varphi = 1$), and the similarity ratio of the strength, cohesion, and elastic modulus is 30 ($C_\sigma = C_c = C_E = 30$). According to the similarity ratio calculation, the physical and mechanical parameters of the model material must be obtained to meet the parameter requirements [31,32]. The similar material ratios of the surrounding rock and its physicomechanical parameters [33] are shown in Tables 1 and 2.

The ratios $C_L = C_\sigma = C_E = 30$ were taken into consideration when formulating lining structural materials. For this lining concrete, the proportion of comparable ingredients was 1:0.9 for water to gypsum. For this test, a monolithic lining model with a 20 cm outside diameter and a 1 cm wall thickness was utilized. Table 3 displays the model and prototype materials for the lining [34].

Table 1. Each constituent material accounted for the mass percentage of similar material in surrounding rock (%).

Iron Powder	Quartz Sand	Barite Powder	Water	Cement
0.204	0.305	0.254	0.136	0.101

Table 2. Physicomechanical parameters of similar materials of surrounding rock.

Index	Prototype Rock	Target Parameter	Measured Parameter
Unit weight γ/(KN·m^{-3})	24.5	24.5	24.5
Strength σ_c/MPa	16.80	0.56	0.55
Elastic modulus E/MPa	4500	150	142
Poisson's ratio μ	0.22	0.22	0.23
Cohesion c/kPa	700–1500	23–50	36
Angle of internal friction φ/(°)	50.0	50.0	41.3

Table 3. Physicomechanical parameters of similar materials of lining structure.

Index	Prototype Material	Target Parameter	Measured Parameter
Strength σ_c/MPa	32.5	1.08	1.10
Elastic modulus E/MPa	34.5	1.15	1.22

The reinforcement of the lining model is built of wire mesh with a diameter of 1.1 mm, which is combined with the design papers of the dependent project tunnels and relevant literature [34,35]. The lining model is developed as a monolithic tube sheet since it is difficult to build in pieces due to its tiny size and brittle gypsum composition. Figure 1 displays the tunnel lining model as well as the lining structure specimens made of similar materials.



Figure 1. Lining structure specimens made of similar materials and tunnel lining model.

2.2. Model Test Device

The main body of the model box, the continuous pressure loading system, and the data acquisition system were all independently designed as part of the model test equipment for the time-dependent investigation of stress and deformation of weak surrounding rock and lining structure in operational tunnels. As shown in Figure 2, the model box body's internal space measures 1.25 m × 1.25 m × 0.3 m.



Figure 2. Model test device.

To achieve the upper pressure and side pressure of the material in the model box for long-lasting, smooth, and constant control and loading, the constant pressure loading system consists of two-force application units that are vertical and horizontal. The force application unit is outfitted with a servo motor elevator to simulate the application of the load.

The major parameters that are monitored during the test are the surrounding rock stress, the internal force and displacement of the lining structure, and the surrounding rock-lining contact force. Figure 3 illustrates the sensor configuration.

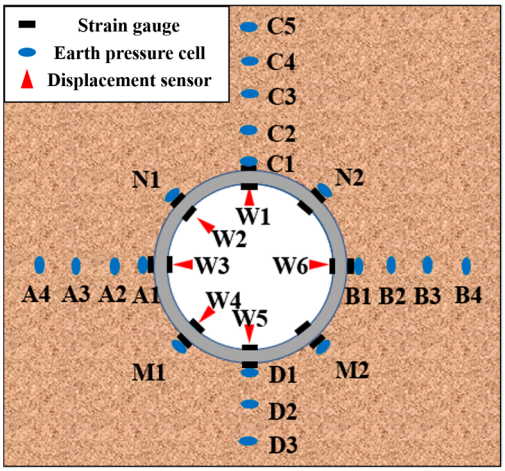


Figure 3. Layout of the data acquisition system.

Earth pressure cells are used to measure the surrounding rock stress and surrounding rock-lining contact force in the tunnel. Beginning at the top of the arch, measuring points are placed every 45° around the ring's perimeter, with eight measuring points per ring. Measuring points are also placed every 10 cm, three horizontally at the arch waist of the lining structure on each side, four vertically upward at the top of the arch, and two vertically downward at the bottom of the arch. Using the formula for determining the internal force of the beam, the strain value determines the internal force of the lining structure. Resistive strain gauges, with 16 measuring points organized in a ring, are placed along the inner and outer sides of the circular lining structure at 45° intervals, starting from the top of the arch. Displacement sensors that are measured inside the lining track the displacement of the lining structure. The displacement sensors are positioned at 45° intervals along the counterclockwise direction within 180° of the top to bottom of the arch, and another symmetrical measuring point is placed at the horizontal position of the right arch waist. The aforementioned monitoring data are gathered using the XL2101G static resistance strain gauge (Produced by Qinhuangdao Xieli Technology Development Co., Qinhuangdao, China) and sent to computer software for data processing, analysis, and storage.

2.3. Experimental Scheme

The design of the model test study program takes into account the tunnel burial depth and the lateral pressure coefficient, which are significant parameters that impact the stress and deformation time-dependent characteristics of the surrounding rock and lining structure. Based on the investigation and design data of the dependent project, the burial depth and lateral pressure coefficient values were determined for the test. Table 4 illustrates how the test conditions are set up. Three conditions for the tunnel burial depth—15, 30, and 45 m—and two types of coefficients for the lateral pressure coefficient—0.3 and 0.5—are chosen.

Table 4. Test conditions.

Condition Number	Simulated Burial Depth/m	Vertical Load/kPa	Lateral Pressure Coefficient	Lateral Load/kPa
1	15	17	0.3	5.1
2	30	31	0.3	9.3
3	45	45	0.3	13.5
4	15	17	0.5	8.5
5	30	31	0.5	15.5

The lateral pressure is maintained constant in working conditions 1–3, and a graded loading mode is used to mimic the variation in tunnel burial depth by varying the loading in the vertical direction. This allows for the study of the impact of burial depth on the time-dependent characteristics of surrounding rock and lining stress and deformation. To study the influence of the lateral pressure coefficient on the time-dependent characteristics of surrounding rock and lining stress and deformation, working conditions 4 and 5 are established, and the graded loading mode is used to simulate the change in lateral pressure coefficient by varying the loading load in the horizontal direction. The loading cycle of each stage of the graded loading mode is set to 8 days because pre-experimental data indicate that the changes in stress and deformation characteristics of the surrounding rock and lining structure after 8 days of loading are very minimal.

The main test steps are as follows: (1) calculating and evaluating the quality of each component material, mixing the materials, and placing the resulting surrounding rock-like material in the model box; (2) creating the tunnel lining structure and burying it as indicated in Figure 4 when the test filler reaches the tunnel's height; (3) installing the data acquisition system in accordance with the test program; (4) waiting for the model to finish laying the overall model before performing the overall maintenance; and (5) following the completion of the maintenance, executing the constant pressure loading test in accordance with the predetermined test program.

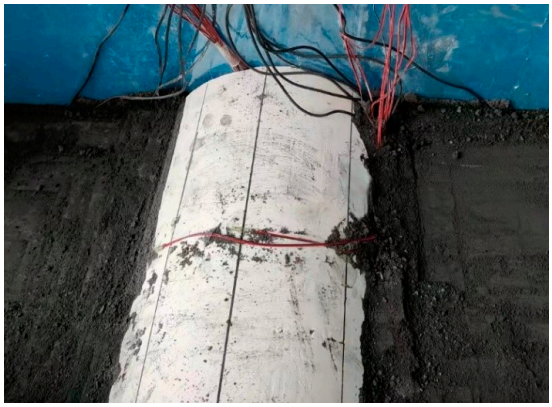


Figure 4. Pre-embedding of tunnel lining structure.

3. Time-Dependent Evolutionary Patterns of Stress and Deformation in Surrounding Rock and Lining Structure

The weak surrounding rock creates a creep effect under environmental pressures during the long-term operation of tunnels, which impacts the long-term operating safety of tunnels by resulting in complicated time-dependent evolutionary patterns of stress and deformation in the surrounding rock and lining. Test group 1 was initially chosen to track changes in the stress of the surrounding rock, the internal force and displacement of the lining structure, and the contact force between the surrounding rock and lining structure in order to analyze the time-dependent evolutionary patterns of stress and deformation of the surrounding rock and lining structure.

3.1. Analysis of Surrounding Rock Stress

Four measurement points were positioned horizontally on the left and right sides of the tunnel arch waist in order to track the radial stress of the surrounding rock in that direction. Figure 5 illustrates the variation in the radial stress of the surrounding rock in that direction at the arch waist. Over time, the surrounding rock stress mostly experiences growth and stabilization phases. The surrounding rock stress grows during a steeply increasing phase that ends with a convex curve after loading. The stress generated by the surrounding rock during loading causes a large, abrupt change in the curve, which is then convex and tends to stabilize. At this point, the surrounding rock stress enters the stabilization phase, and the curve continues to change slowly over time while the stress of the surrounding rock increases and the growth rate is small. This demonstrates how the surrounding rock stress has a time-dependent feature that changes over time as a result of the creep effect of the surrounding rock. Additionally, in the horizontal direction at the tunnel's arch waist, the stress initially rises and subsequently falls with an increase in radial distance; the sizes of the stress on the left and right sides are almost equal, and the rule of change is also consistent.

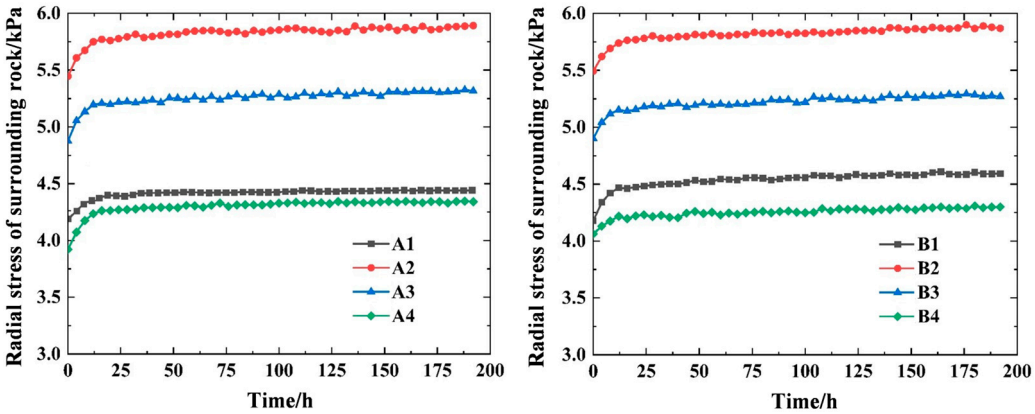


Figure 5. Variation of radial stress of surrounding rock in horizontal direction at arch waist. (**a**) Left measurement point; (**b**) Right measurement point.

Five measurement points were positioned vertically at the top of the tunnel arch and three at the bottom of the arch to track the radial stress of the surrounding rock in the vertical direction. Figure 6 illustrates the change in the radial stress of the surrounding rock in the vertical direction. It is comparable to the horizontal trend of surrounding rock radial stress at the arch waist, and over time, the surrounding rock stress primarily moves through the growth and stabilization stages. Additionally, it demonstrates how the surrounding rock stress changes over time due to the creep effect of the surrounding rock. The magnitudes of the upper and lower sides of the stress are almost equal, and the rule of change is consistent as the stress drops in the vertical direction with an increase in radial distance.

3.2. Analysis of Internal Force and Displacement of Lining Structure

A total of 16 measurement sites were placed on the inner and outer surfaces of the liner model in order to track the internal force of the lining structure. Figure 7 illustrates the internal force imparted to the lining structure. Among these, compression produces a positive axial force, while tension on the lining's outer surface and compression on its inner surface provide a positive bending moment. The loading moment, midway moment, and end moment of the test are represented by the values of t = 0, 98, and 196 h, respectively. The lining's maximal axial force, 196.1 kN, is found at the left arch's waist. The lining's internal force is essentially spread symmetrically from left to right and up and

down. The entire lining is under pressure. The top of the arch experiences the greatest bending moment, which is 25.0 kN·m (absolute), whereas the upper and lower arch girdles experience essentially no bending. The outside surface of the lining is tensile at both sides of the arch girdle, and the bottom and top of the arch are pressured. The axial force increases from the middle moment to the ending moment and from the loading moment to the middle moment, respectively, and is stronger at all points along the lining at the ending moment than at the loading moment. Consequently, it suggests that the creep effect of the surrounding rock has a time-dependent characteristic that causes the internal force of the lining structure to change over time.

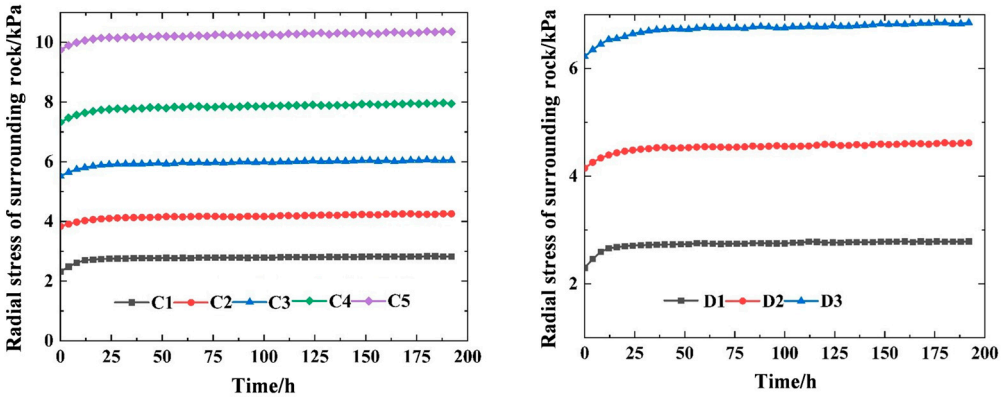


Figure 6. Variation of radial stress of surrounding rock in vertical direction. (**a**) Top measurement point; (**b**) Bottom measurement point.

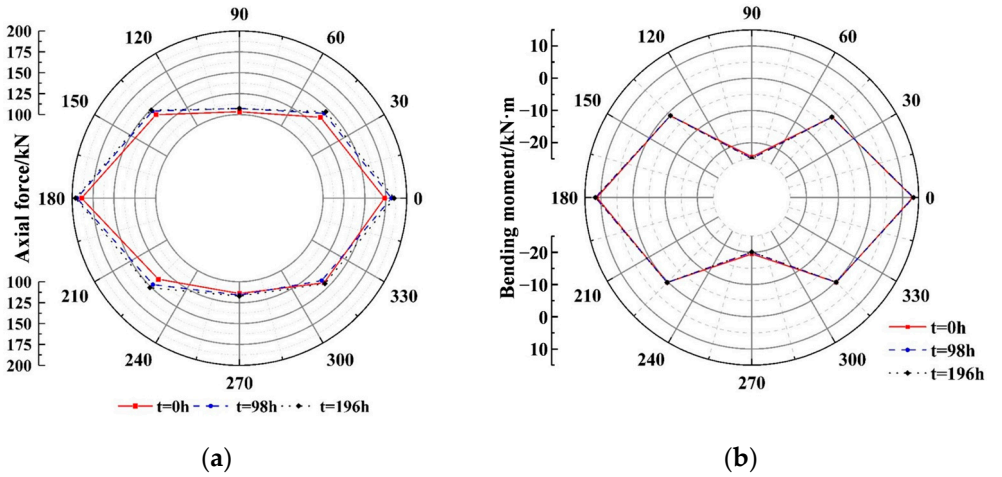


Figure 7. Internal force of lining structure. (**a**) Axial force; (**b**) Bending moment.

Six measuring stations were positioned inside the lining structure to track its displacement; the displacement of the lining structure is depicted in Figure 8. The tunnel's inner lining deformation is seen as a positive direction of deformation. Over time, the displacement of every position in the lining structure primarily goes through two stages: deformation and stability. Every curve in the deformation stage mutates initially and then tends to stabilize, with the exception of the left and right arch waists, where the deformation protrudes outward; at all other points, the deformation occurs to the interior. The vault experienced the greatest displacement of 1.50 mm out of all the locations where the lining structure was present. While the displacements at the foot and bottom of the arch decreased over time as a result of the surrounding rocks settling, the displacements at the top of the arch and the left and right arch waists increased over time, but the growth rate eventu-

ally slowed and reached a stable state. As the test came to a close, displacement varied at every site in comparison to the instantaneous displacement in the deformation stage, with the maximum displacement increment being 0.39 mm. This suggests that the lining displacement likewise possesses the time-dependent characteristic of changing over time.

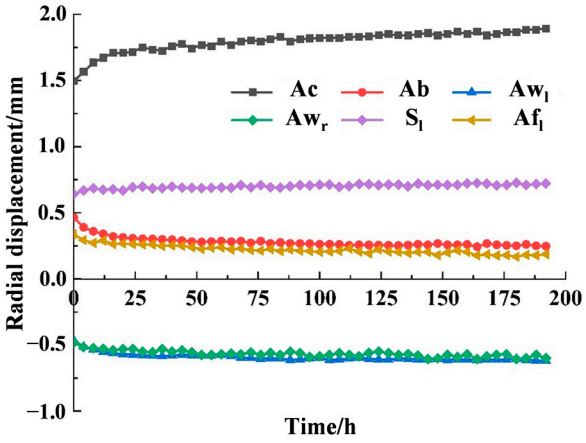


Figure 8. Radial displacement of lining structure (Ac for arch crown, Ab for arch bottom, Aw_l for left arch waist, Aw_r for right arch waist, S_l for left spandrel, Af_l for left arch foot).

3.3. Analysis of Contact Force between Surrounding Rock and Lining Structure

Eight measurement points were placed on the surrounding rock and lining contact surface to track the surrounding rock-lining contact force. The contact force between the surrounding rock and lining structure is pressure, and it varies, as Figure 9 illustrates. This change's trend is comparable to the surrounding rock's radial stress in the horizontal direction at the arch waist in Section 3.1. As time goes on, the surrounding rock-lining contact force primarily goes through the deformation stage and the stabilization stage. It also demonstrates how the surrounding rock's creep effect causes the rock-lining contact force to change over time, exhibiting a time-dependent characteristic. The lining structures were subjected to the pressure of the surrounding rock in the following order: left and right arch waist > left and right spandrel > left and right arch foot > arch crown > arch bottom. However, when the pressure increment was calculated as a percentage of the instantaneous pressure at the time of loading, the right arch waist had the smallest incremental proportion and the left and right arch top the largest.

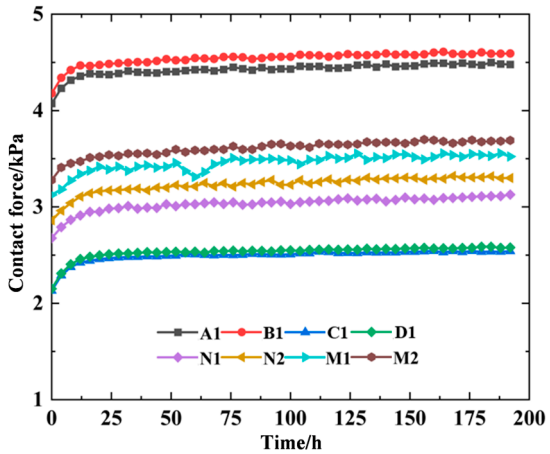


Figure 9. Contact force between surrounding rock and lining structure.

4. Analysis of Factors Influencing the Time-Dependent Characteristics of Stress and Deformation in Surrounding Rock and Lining Structure

4.1. Influence of Burial Depth on Time-Dependent Characteristics of Stress and Deformation in Surrounding Rock and Lining Structure

The stress and deformation of the surrounding rock and lining are significantly influenced by the burial depth (d_b), and the time-dependent characteristics of the stress and deformation of the surrounding rock and lining may differ depending on the burial depth. At burial depths of 15, 30, and 45 m, the time-dependent characteristics of stress and deformation in the surrounding rock and lining structure are examined when the lateral pressure coefficient is 0.3. The surrounding rock stress, the internal force and displacement of the lining structure, and the surrounding rock-lining contact force are all monitored during the model test.

Figures 10 and 11 illustrate how the surrounding rock stress varies under different burial depth conditions. The surrounding rock stress fluctuates sharply in response to changes in burial depth before gradually stabilizing over time. The surrounding rock stress increases as tunnel depth increases, and the time-dependent characteristics of these changes become more evident. As an illustration, consider the monitoring point A1 in Figure 10. The load retention process caused the radial pressure to increase by 0.41 kPa at a tunnel depth of 15 m, and at a tunnel depth of 45 m, it increased by 2.07 kPa. The time-dependent characteristics of stress and deformation in surrounding rock and lining are significantly influenced by the tunnel burial depth. The three types of burial depth conditions of surrounding rock stress, as well as the 3.1 section of surrounding rock stress, are consistent in terms of size and distribution. As the radial distance grows, the surrounding rock stress increases vertically, climbs, and then falls horizontally, and on both sides, the stress size and distribution change symmetrically in both vertical and horizontal directions.

Figure 12 illustrates how the surrounding rock-lining contact force varies under various burial depth circumstances. Similar to the surrounding rock-lining contact force in Section 3.3, the surrounding rock pressure on each portion of the lining under varying burial depths follows the same order, which is likewise left and right arch waist > left and right spandrel > left and right arch foot > arch top > arch bottom. When compared to the force at the same location at a burial depth of 30 m, the surrounding rock-lining contact force at the left arch girdle increased significantly at 45 m. Similarly, the force at the right arch waist increased significantly by approximately 4.7 kPa, and the pressure increment at the remaining locations increased as the burial depth increased.

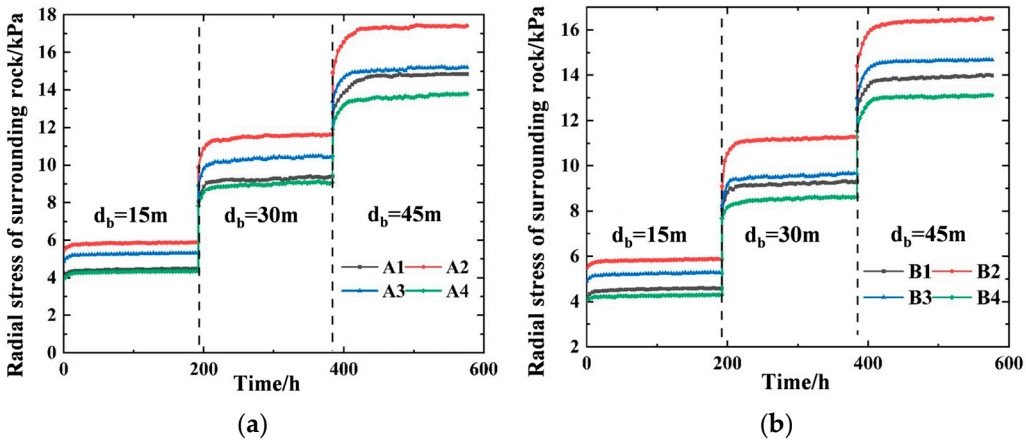


Figure 10. Variations in the surrounding rock's horizontal radial tension at the arch waist of the tunnel with varying burial depths. (**a**) Left measurement point; (**b**) Right measurement point.

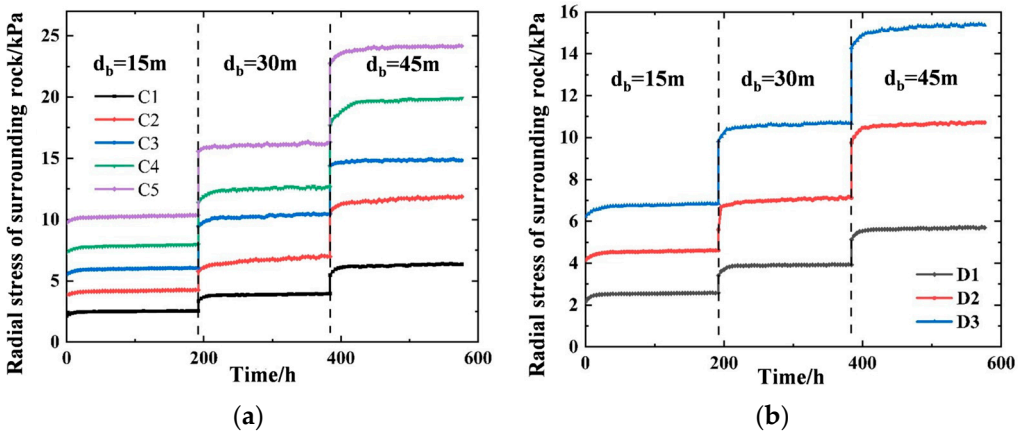


Figure 11. Variation in the vertical direction of the radial stress in the tunnel surrounding rock at varying burial depths. (**a**) Top measurement point; (**b**) Bottom measurement point.

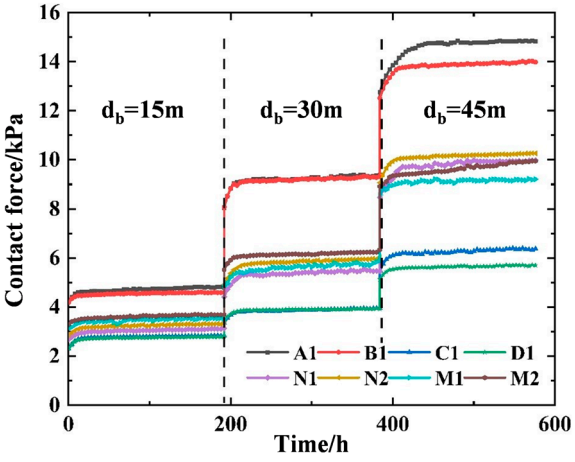


Figure 12. Variation of surrounding rock-lining contact force under different burial depths.

Based on the aforementioned analysis, the loading method of grading three times is used to simulate the change in tunnel depth. As a result, there are three stages of changes in the surrounding rock stress and the surrounding rock-lining contact force, and each stage has growth and stabilization stages of the stress. The growth stage is the process of the curve increasing steeply after loading to the point where the curve shows a convex process. The curve initially changes dramatically upon loading, which is caused by the surrounding rock producing stress and rapid growth during the loading moment. Afterward, the curve tends to convex and stabilize, bringing the surrounding rock stress into the stabilization stage. This demonstrates that both the surrounding rock stress and the surrounding rock-lining contact force have the time-dependent characteristic of changing with time due to the creep effect of the surrounding rock. Additionally, as burial depth increases, not only does the stress increase, but its time-dependent characteristic becomes more evident.

Figure 13 illustrates how the lining's displacement changes depending on the burial depth. At each stage, there was an abrupt change in the displacements, which later increased over time, but the growth rate slowed down and eventually reached the steady creep stage. The left and right arch waists exhibit the least amount of deformation, while the arch crown experiences the most deformation. At a burial depth of 30 m, the arch crown exhibits 3.81 mm of deformation, and at a depth of 45 m, this location experiences 6.29 mm of deformation. These findings demonstrate the significant impact of burial depth on the time-dependent variation of the lining displacement, leading to a continuously fluctuating deformation over time.

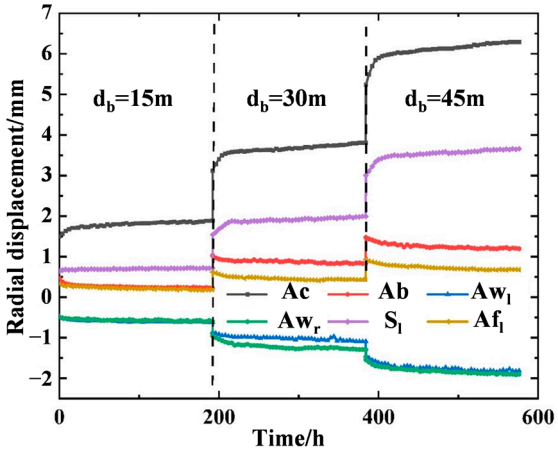
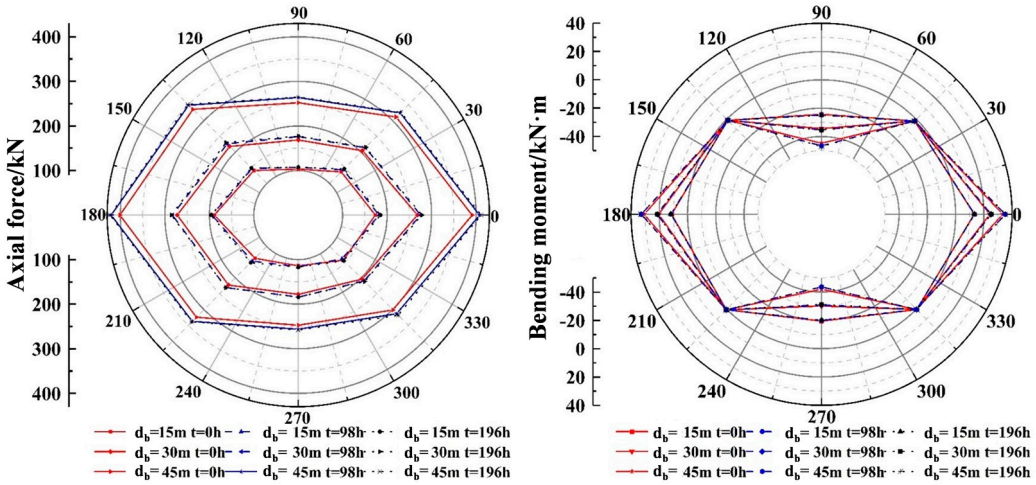


Figure 13. Variation of radial displacement of lining structure under different burial depths (Ac for arch crown, Ab for arch bottom, Aw_l for left arch waist, Aw_r for right arch waist, S_l for left spandrel, Af_l for left arch foot).

Figure 14 illustrates how the internal force of the lining structure varies at various burial depths. At 15 and 30 m below ground, the axial force increment ranges are 3–10 kN and 6–13 kN, respectively, and the absolute value of the bending moment increment at the arch crown is 0.60 kN·m and 0.98 kN·m, respectively. These results demonstrate that as tunnel depth increases, so does the internal force of the lining, and the time-dependent characteristics of these changes become more apparent. At the arch foot and spandrel, the bending moment is nearly zero, and the variation is negligible.



(**a**) (**b**)

Figure 14. Internal force of lining structure under different burial depths. (**a**) Axial force; (**b**) Bending moment.

4.2. Influence of Lateral Pressure Coefficient on Time-Dependent Characteristics of Stress and Deformation in Surrounding Rock and Lining Structure

The stress and deformation of the surrounding rock and lining are significantly influenced by the lateral pressure coefficient (c_{lp}), and the time-dependent characteristics of the stress and deformation of the surrounding rock and lining may differ depending on the lateral pressure coefficient. In this model test, the impact of changing the loads loaded in the horizontal direction by setting up conditions 4 and 5 based on conditions 1 and 2 was realized by altering the surrounding rock stress, internal force and displacement of the lining structure, and surrounding rock-lining contact force.

Figures 15 and 16 illustrate how the surrounding rock stress changes under various lateral pressure coefficient circumstances. The surrounding rock stresses at all measurement points, with the exception of A1 and B1, increased significantly in the horizontal direction after the lateral pressure coefficient was changed from 0.3 to 0.5, while they slightly decreased at A1 and B1. The instantaneous stresses at measurement points A1, A2, A3, and A4 at a lateral pressure coefficient of 0.5 and a lateral pressure coefficient of 0.3 differ at the first moment of load application by −0.22, 2.24, 2.26, and 2.75, respectively, and at measurement points B1, B2, B3, and B4 by −0.32, 2.43, 2.17, and 2.53, respectively. The changes in the surrounding rock stress were minimal in the vertical direction. A range of stress-reduction zones forms near the tunnel's horizontal direction as a result of the surrounding rock's lower strength and larger compressive stress concentration. Using Figure 15a as an example, the monitoring point A1 is located in this zone, and as a result, its surrounding rock stress is lower than that of the monitoring points A2, A3, and A4.

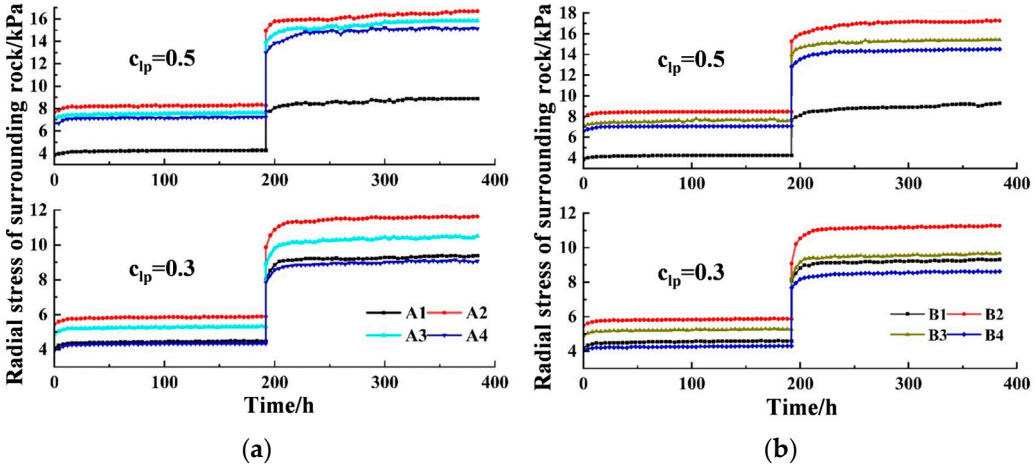


Figure 15. Variations in the surrounding rock's horizontal radial tension at the arch waist of the tunnel with varying lateral pressure coefficients. (**a**) Left measurement point; (**b**) Right measurement point.

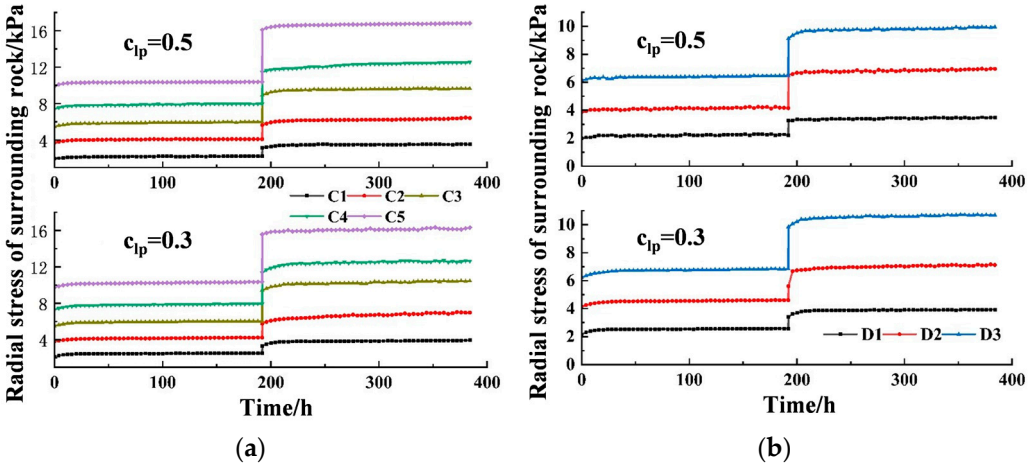


Figure 16. Variation in the vertical direction of the radial stress in the tunnel surrounding rock at varying lateral pressure coefficients. (**a**) Top measurement point; (**b**) Bottom measurement point.

Figure 17 illustrates how the surrounding rock-lining contact force changes with varying lateral pressure coefficients. In accordance with the law of the contact force of surrounding rock and lining in Section 3.3, the lining structure is subjected to the pressure of surrounding rock in the following order when two different lateral pressure coefficients are used: left and right arch waist > left and right spandrel > left and right arch foot > arch crown > arch bottom. The pressure of the surrounding rock at the six measurement places

reduces with a change in the lateral pressure coefficient, and this also results in a drop in the pressure increment during the stabilization stage. It is evident that the lateral pressure coefficient lessens the force acting on the lining structure and has a significant impact on the lining force action.

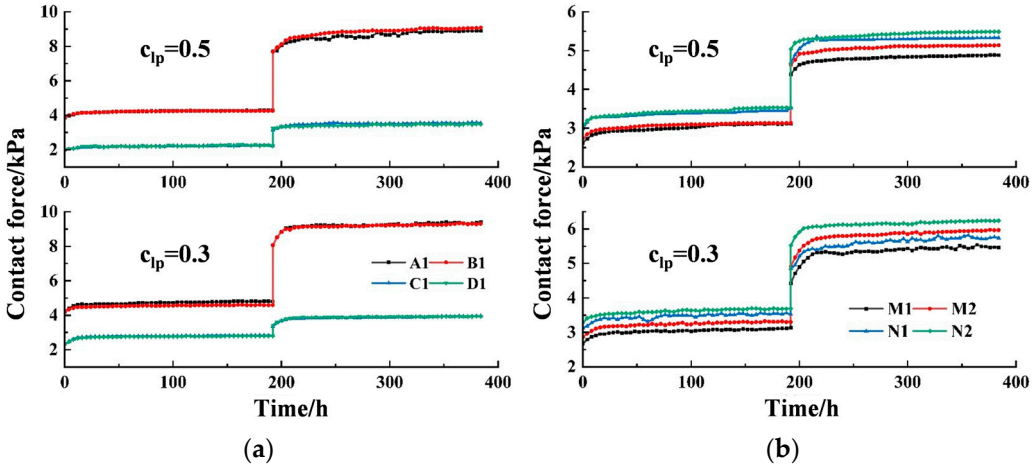


Figure 17. Variation of surrounding rock-lining contact force under different lateral pressure coefficients. (**a**) Measuring points at the top, waist, and bottom of the arch in the tunnel; (**b**) Measuring points at the spandrel and arch foot in the tunnel.

Figure 18 depicts the lining structure's radial displacement changes under various lateral pressure coefficients. The largest deformation happens at the arch crown when two distinct lateral pressure coefficients are utilized. The displacements of each measurement point decreased to varying degrees as the lateral pressure coefficient increased. This indicates that the lateral pressure coefficient plays a significant role in the tunnel structure's safety and that increasing the lateral pressure coefficient is beneficial for reducing the deformation of the tunnel lining structure.

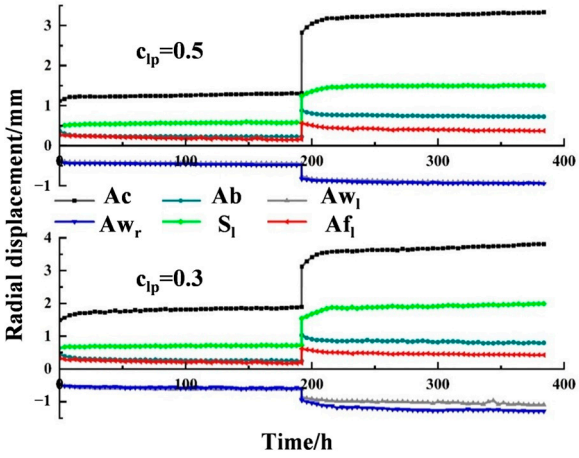
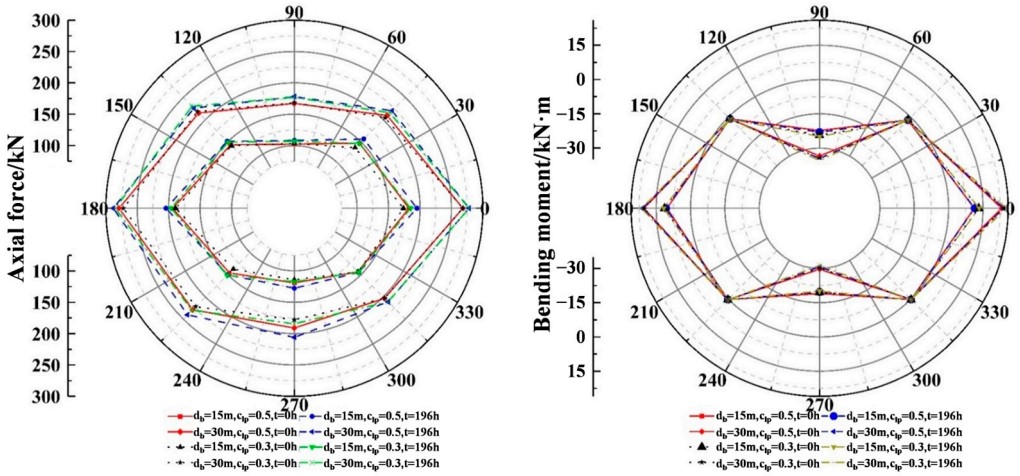


Figure 18. Variation of radial displacement of lining structure under different lateral pressure coefficients (Ac for arch crown, Ab for arch bottom, Aw_l for left arch waist, Aw_r for right arch waist, S_l for left spandrel, Af_l for left arch foot).

Figure 19 illustrates how the lining structure's internal force varies under various lateral pressure coefficients. When the lateral pressure coefficient is between 0.3 and 0.5 at a burial depth of 15 m, the incremental range of axial force at each position is 3–10 kN and 4–12 kN, respectively. This indicates that as the lateral pressure coefficient increases, the axial force of the lining increases as well, and the time-dependent characteristic of the axial force of the lining becomes more evident. Additionally, the bending moment change

does not follow the axial force change rule. As the lateral pressure coefficient increases, the absolute value of the bending moment appears to decrease to varying degrees throughout the rest of the position, with the exception of the left and right arch foot and spandrel at the bending moment throughout nearly 0.



(**a**) (**b**)

Figure 19. Internal force of lining structure under different lateral pressure coefficients. (**a**) Axial force; (**b**) Bending moment.

5. Conclusions and Discussion

The model test of surrounding rock and lining structure stress and deformation time-dependent characteristics was conducted based on the creep effect of weak surrounding rock medium. The stress and deformation time-dependent characteristics of operational tunnels under various burial depths and lateral pressure coefficients were examined. The following are the paper's conclusions and discussion:

1. By examining the stress and deformation of the surrounding rock and lining structure over time, one can observe that, as long as the load remains constant, the surrounding rock's stress, the lining structure's internal force and displacement, and the contact force between the lining and surrounding rock all increase over time and eventually tend to stabilize. It suggests that the surrounding rock and lining structure's stress and deformation have an evolutionary characteristic that changes with time;
2. When the radial distance increases in a vertical direction, the surrounding rock stress reduces, whereas, in a horizontal direction, the surrounding rock stress increases and then declines. The stress size and pattern of change on both sides of the tunnel are nearly the same, regardless of whether the orientation of the forces is vertical or horizontal. With the exception of the left and right arch waists, where the deformation protrudes outward, the lining structure deforms quickly under pressure. All other positions experience internal distortion, with the arch top experiencing the greatest amount of deformation. In accordance with the lining structure's surrounding rock pressure, which goes from large to small order: Left and right arch waist > left and right spandrel > left and right arch foot > arch top > arch bottom;
3. The surrounding rock stress, lining structure internal force, and surrounding rock and lining structure contact force all increase as tunnel burial depth increases, making the time-dependent characteristics of the change more evident. Burial depth also has a significant impact on the lining deformation of the time-dependent changes, with the arch top consistently experiencing the greatest deformation;
4. Increases in the lateral pressure coefficient have a significant effect on the surrounding rock stress in the horizontal direction while having little effect on the vertical direction. Additionally, the lateral pressure coefficient has a significant influence on the axial

force of the lining structure, the bending moment and displacement of the lining, and the contact force between the surrounding rock and the lining, all of which experience varying degrees of reduction. These findings suggest that the lateral pressure coefficient plays a critical role in the long-term safety of the tunnel structure and that an increase in the lateral pressure coefficient is beneficial to the control of the stress and deformation of the tunnel lining structure;

5. The stress and deformation evolution of the surrounding rock and lining during long-term tunnel operation and maintenance has been obtained in this study, which can offer theoretical references for the identification of the operational tunnels' service state as well as for the prediction, prevention and control of diseases. However, the monitoring period of the model tests should be extended in subsequent studies in order to obtain more comprehensive experimental data on the long-term behavior of the surrounding rock and lining structure. This will allow for the detection of trends and evolutionary patterns that may be missed in shorter monitoring periods, which could serve as a foundation for a more robust and reliable tunnel design approach.

Author Contributions: Conceptualization, P.W. and X.M.; methodology, L.Y.; validation, L.Y., X.S. and X.W.; investigation, P.W.; resources, L.Y.; data curation, X.M.; writing—original draft preparation, P.W.; writing—review and editing, X.M. and L.Y.; visualization, C.L.; supervision, L.Y. All authors have read and agreed to the published version of the manuscript.

Funding: This research was funded by the National Key Research and Development Program of China (grant number 2021YFB2600800), the Key Research Program of Yunnan Province, China (grant number 202103AA080016), and the National Natural Science Foundation of China (grant number 52178338).

Institutional Review Board Statement: Not applicable.

Informed Consent Statement: Not applicable.

Data Availability Statement: Data are contained within the article.

Acknowledgments: The authors would like to thank the editors and anonymous reviewers for their valuable and constructive comments related to this manuscript.

Conflicts of Interest: Author Xujin Ma was employed by Hubei Provincial Tendering Co., Ltd.. The remaining authors declare that the research was conducted in the absence of any commercial or financial relationships that could be construed as a potential conflict of interest.

References

1. Editorial Department of China Journal of Highway and Transport. Review on China's traffic tunnel engineering research: 2022. *China J. Highw. Transp.* **2022**, *35*, 1–40.
2. Han, B.; Xi, Z.; Sun, Y.; Lu, F.; Niu, C.; Wang, C.; Xu, K.; Yao, Y. Statistical analysis of urban rail transit operation in the world in 2022: A review. *Urban Rapid Rail Transit* **2023**, *36*, 1–8.
3. Liu, C.; Zhang, D.; Zhang, S.; Sun, Z. Interaction analysis between composite supports and rheological rock considering progressive hardening characteristic of shotcrete. *Constr. Build. Mater.* **2023**, *374*, 130876. [CrossRef]
4. Einstein, H.H.; Schwartz, C.W. Simplified analysis for tunnel supports. *J. Geotech. Eng. Div.* **1979**, *105*, 499–518. [CrossRef]
5. Yu, X.; Zheng, Y.; Liu, H. *Stability Analysis of Underground Engineering Surrounding Rock*, 1st ed.; Coal Industry Press: Beijing, China, 1983; pp. 11–20.
6. Li, S.; Wang, M. Elastic analysis of stress–displacement field for a lined circular tunnel at great depth due to ground loads and internal pressure. *Tunn. Undergr. Space Technol.* **2008**, *23*, 609–617. [CrossRef]
7. Lu, A.; Zhang, L.; Zhang, N. Analytic stress solutions for a circular pressure tunnel at pressure and great depth including support delay. *Int. J. Rock Mech. Min.* **2011**, *48*, 514–519. [CrossRef]
8. Carranza-Torres, C.; Rysdahl, B.; Kasim, M. On the elastic analysis of a circular lined tunnel considering the delayed installation of the support. *Int. J. Rock Mech. Min.* **2013**, *61*, 57–85. [CrossRef]
9. Fang, H.; Zhang, D.; Fang, Q.; Wen, M. A generalized complex variable method for multiple tunnels at great depth considering the interaction between linings and surrounding rock. *Comput. Geotech.* **2021**, *129*, 103891. [CrossRef]
10. Zhou, Z.; He, C.; Chen, Z.; Wang, B.; Li, T.; Jiang, C. Analysis of interaction mechanism between surrounding rock and supporting structures for soft-rock tunnels under high geo-stress. *Acta Geotech.* **2023**, *18*, 4871–4897. [CrossRef]

11. Lu, Q.; Xiao, Z.; Ji, J.; Zheng, J.; Shang, Y. Moving least squares method for reliability assessment of rock tunnel excavation considering ground-support interaction. *Comput. Geotech.* **2017**, *84*, 88–100. [CrossRef]
12. Zhao, N.; Shao, Z.; Chen, X.; Yuan, B.; Wu, K. Prediction of mechanical response of "a flexible support system" supported tunnel in viscoelastic geomaterials. *Arch. Civ. Mech. Eng.* **2022**, *22*, 160. [CrossRef]
13. Du, C.; Zhou, C.; Jiang, N.; Huang, Y. Structural stability monitoring of model test on highway tunnel with lining backside voids using dynamic and static strain testing sensors. *Sensors* **2023**, *23*, 1403. [CrossRef] [PubMed]
14. Xu, Z.; Luo, Y.; Chen, J.; Su, Z.; Zhu, T.; Yuan, J. Mechanical properties and reasonable proportioning of similar materials in physical model test of tunnel lining cracking. *Constr. Build. Mater.* **2021**, *300*, 123960. [CrossRef]
15. Wu, H.; Fan, F.; Yang, X.; Wang, Z.; Lai, J.; Xie, Y. Large deformation characteristics and treatment effect for deep bias tunnel in broken phyllite: A case study. *Eng. Fail. Anal.* **2022**, *135*, 106045. [CrossRef]
16. Hu, Z.; Shen, J.; Wang, Y.; Guo, T.; Liu, Z.; Gao, X. Cracking characteristics and mechanism of entrance section in asymmetrically-load tunnel with bedded rock mass: A case study of a highway tunnel in southwest China. *Eng. Fail. Anal.* **2021**, *122*, 105221. [CrossRef]
17. Yang, L.; Sheng, X.; Zhang, B.; Yu, H.; Wang, X.; Wang, P.; Mei, J. Propagation behavior of hydraulic fractures in shale under triaxial compression considering the influence of sandstone layers. *Gas Sci. Eng.* **2023**, *110*, 204895. [CrossRef]
18. Sheng, X.; Yang, L.; Wang, T.; Zhou, X.; Yu, H.; Zhang, Y.; Fu, X.; Mei, J.; Pei, Y. Hydraulic fracturing behavior of shale-sandstone interbedded structure under true triaxial stress conditions: A comprehensive experimental analysis. *Fatigue Fract. Eng. Mater. Struct.* **2024**, *47*, 1246–1261. [CrossRef]
19. Cui, G.; Wang, X.; Wang, D. Study on the model test of the antibreaking effect of fiber reinforced concrete lining in tunnel. *Shock Vib.* **2020**, *2020*, 5419650. [CrossRef]
20. Wang, D.; Qi, J.; Cui, G.; Yang, Y.; Chang, J. Model test on bearing characteristics of basalt fiber-reinforced concrete lining. *Adv. Mater. Sci. Eng.* **2020**, *2020*, 3891343. [CrossRef]
21. Qiu, J.; Zhou, X.; Shen, Y.; Zhang, X.; Yu, B.; Luo, Y. Failure mechanism of the deep-buried metro tunnel in mixed strata: Physical model test and numerical investigation. *Tunn. Undergr. Space Technol.* **2023**, *139*, 105224. [CrossRef]
22. Li, P.; Xie, S.; Yang, X.; Wang, Z.; Wang, S. Investigation into the construction response of tunnels through fault: Model test. *Appl. Sci.* **2023**, *13*, 4460. [CrossRef]
23. Zhou, J.; Yang, X.; Chu, Z. Load laws of composite lining in mountain tunnel model tests and numerical simulation validation. *J. Mt. Sci.* **2023**, *20*, 2041–2057. [CrossRef]
24. Ma, Y.; Wang, Z.; Wang, D. The safe load-bearing capacity of railway tunnel linings under high-pressure and water-rich conditions. *Buildings* **2023**, *13*, 2154. [CrossRef]
25. Liu, C.; Zhang, D.; Zhang, S. Characteristics and treatment measures of lining damage: A case study on a mountain tunnel. *Eng. Fail. Anal.* **2021**, *128*, 105595. [CrossRef]
26. Lu, P.; Qiao, D.; Wu, C.; Wang, S.; He, X.; Zhang, W.; Zhou, H. Effect of defects and remediation measures on the internal forces caused by a local thickness reduction in the tunnel lining. *Undergr. Space* **2022**, *7*, 94–105. [CrossRef]
27. Jia, S.; Wen, C.; Wu, B. A nonlinear elasto-viscoplastic model for clayed rock and its application to stability analysis of nuclear waste repository. *Energy Sci. Eng.* **2020**, *8*, 150–165. [CrossRef]
28. Ren, L.; Wei, Z.; Liang, N.; Liu, X.; Deng, Z. Mechanical behavior of multi-scale fiber-reinforced concrete for secondary tunnel lining: Field test and numerical simulation. *Case Stud. Constr. Mat.* **2022**, *17*, e01669. [CrossRef]
29. Ren, M.; Wu, X.; Pan, J.; Liu, H.; Li, N. Theoretical and numerical studies of rock-support interaction by considering imperfect rock-lining interface. *Geotech. Geol. Eng.* **2023**, *41*, 1741–1762. [CrossRef]
30. Fan, X.; Yang, Z.; Li, K. Effects of the lining structure on mechanical and fracturing behaviors of four-arc shaped tunnels in a jointed rock mass under uniaxial compression. *Theor. Appl. Fract. Mech.* **2021**, *112*, 102887. [CrossRef]
31. Wang, H.; Li, S.; Zhang, Q.; Li, Y.; Guo, X. Development of a new geomechanical similar material. *Chin. J. Rock Mech. Eng.* **2006**, *25*, 1842–1847.
32. Li, S.; Zhou, Y.; Li, L.; Zhang, Q.; Song, S.; Li, J.; Wang, K.; Wang, Q. Development and application of a new similar material for underground engineering fluid-solid coupling model test. *Chin. J. Rock Mech. Eng.* **2012**, *31*, 1128–1137.
33. Ma, X. Study on Long-Term Interaction Law Between Surrounding Rock and Segment Structure of Shield Tunnel Considering Creep Effect of Rock Mass. Master's Thesis, Shandong University, Jinan, China, 2023.
34. Wang, S.; Shen, X.; He, X.; Yao, J. A model test for the mechanical property and failure mode of lining segments with different assembly types of shield tunnel. *Chin. Civ. Eng. J.* **2017**, *50*, 114–124.
35. Tian, C. Study on Load Distribution Law of Shield Tunnel in Foshan Soft Clay Layer. Master's Thesis, Chang'an University, Xi'an, China, 2020.

Disclaimer/Publisher's Note: The statements, opinions and data contained in all publications are solely those of the individual author(s) and contributor(s) and not of MDPI and/or the editor(s). MDPI and/or the editor(s) disclaim responsibility for any injury to people or property resulting from any ideas, methods, instructions or products referred to in the content.